An investigation of drug compact topography as relates to intrinsic dissolution rates determined by dissolution imaging

Benedict Brown[a,b], Zayeem Fazili[a,b], Adam Ward[a], Karl Walton[b], Liam Blunt[b], Jesper Østergaard[c], Kofi Asare-Addo[a]*,

[a]Department of Pharmacy, University of Huddersfield, Huddersfield, HD1 3DH, UK

[b]EPSRC Future Metrology Hub, University of Huddersfield, Huddersfield, HD1 3DH, UK

[c]Department of Pharmacy, University of Copenhagen, Universitetsparken 2, DK-2100 Copenhagen, Denmark

*Corresponding author (Kofi Asare-Addo)

e-mail: k.asare-addo@hud.ac.uk

Tel: +44 1484 472360

Fax: +44 1484 472182

Submission: JDDST

Abstract

The purpose of this study was to characterize compact surfaces (surface roughness) and study its potential importance to the intrinsic dissolution rate (IDR) as determined by dissolution imaging. To this end, the effect of varying compaction pressures and the use of two stainless-steel surfaces with different textures/roughness on the intrinsic dissolution were investigated. Ketoprofen (KET), paracetamol (PAR) and ibuprofen (IBU) were compacted and a focus variation microscope used to determine the surface topology of the compacts. IDR determination was conducted using a surface dissolution imaging apparatus with the flow-through set up in phosphate buffer at pH 7.2 and 37 °C. The results indicated a general decrease in the surface area of the drug compacts with an increase in compaction force, p values < 0.05 for IBU and PAR but not KET. This change in surface area was measured using the *Sdr* parameter, which can be defined as the developed interfacial area. The smoother stainless-steel plate insert produced significantly smoother compacts for KET (*Sdr* decreased from 0.30 % to 0.07 %). However, PAR and IBU compacts showed an increase in their *Sdr* values from 3.94 % to 17.90 % and from 0.60 % to 0.83 %, respectively, suggesting the changes in surface properties to be drug specific relating to poor compaction properties and elasticity. The dissolution studies suggested that low compaction forces were not suitable for PAR. Overall changes in the surface topology did not have a significant effect on the obtained IDR values.

Keywords: Ketoprofen, paracetamol, ibuprofen, intrinsic dissolution rate, UV-imaging, focus variation microscopy, dissolution imaging

Abbreviations: NCE, new chemical entity; API, active pharmaceutical ingredient; BCS, biopharmaceutical classification system; SDI, surface dissolution imaging; IDR, Intrinsic dissolution rate; KET, ketoprofen; PAR, paracetamol; IBU, Ibuprofen; XRPD, X-ray powder diffraction

Introduction

The need to reduce the cost and time from the identification of a new chemical entity (NCE) to its eventual dosage form is of great importance in the pharmaceutical industry. The Biopharmaceutical classification system (BCS) is used to classify compounds (1, 2) according to their solubilities and permeation behaviour. For some compounds, solubility alone has been shown to be a poor predictor of in-vivo drug performance (3, 4), thus, to guide formulation development, dissolution (rate) is frequently determined (5). Traditional compendial dissolution testing instrumentation requires a relatively large amount of compound. As the amount of compound available at early stage development is limited, these compendial dissolution methods are often not suitable (6, 7).

In the context of the BCS solubility classification, highly soluble APIs have been suggested to possess intrinsic dissolution rates above 0.1 $mg\,min^{-1}\,cm^{-2}$, whereas rates below this limit would often be attributed to APIs with a low BCS solubility classification (8). Albeit a seemingly simple parameter, the determination of intrinsic dissolution rates remains challenging (9, 10). Intrinsic dissolution rate (IDR), the rate of dissolution adjusted for the surface area of a compound (e.g., µg/min/cm^2), is measured while controlling the surface area available for dissolution and applying sink conditions (5, 9). Factors, such as the hydrodynamics, can affect IDR measurements as IDR is not an absolute drug property (11). Asides from experimental setup variations such as hydrodynamics, variation in drug compacts surface area may also cause increases in variation of drug IDR; particularly when compact homogeneity is a concern (12). In IDR determination utilizing miniaturized, sample sparing set-ups, the control of compact surface properties becomes even more important. Loosely attached API particles on the surface of compacts may give rise to erroneous data, for this reason, in some studies data from the beginning of the experiment are excluded (7, 13, 14). The Miniaturised INtrinsic DISsolution screening (MINDISS) assay (13), the µDISS Profiler (15,

16), the Partially Automated Solubility Screening (PASS) assay (17), the miniaturized assay for solubility and residual solid screening (SORESOS) (18), the SiriusT3 and inForm are compound sparing techniques developed for IDR determination (5).

Surface Dissolution Imaging (SDI) instrumentation with Actipix™ Technology (Sirius Analytical now Pion) offers a UV-Vis imaging platform and a compound sparing approach that has been used for determining IDRs (7, 14, 19-25). This flow-through based technique typically requires 5–10 mg of API with an experimental run time of 20–30 min for IDR determination. UV imaging has also been useful in other applications, such as biorelevant characterisation of salts, solid dispersions, transdermal patches, and hydrogels (26-36). Alongside, the potential of the technique in relation to quality control assessment has been suggested (20, 34, 37).

The use of complementary imaging to inspect drug compacts prior to IDR determination is not a new concept, both qualitative and quantitative approaches have been used previously. Madelung et al. utilised SEM and SEM-EDX to detect surface inhomogeneities on the API discs potentially affecting dissolution behaviour (38). Alsenz et al. used optical microscopy to inspect compacts prior to IDR determination (11). Hiew et al. also used optical microscopy, but however gained quantitative data with the attachment of a Raman spectrometer. This combination was used to analyse drug content of drug-excipient compacts prior to IDR determination with an Actipix SDI 300 (39). Focus variation microscopy has also been employed to suggest that rough drug compact surfaces, may increase the variation of IDR measurements (14, 34, 35).

The primary aim of this research was to study the importance of drug compact preparation and properties on the consistency/variability of intrinsic dissolution rate measurements. This aim was explored by firstly varying the compression pressure and secondly, varying the surface which the drug powder was compacted against by manufacturing a relatively “smoother” plate insert. Four different compaction forces were investigated to determine their effect on the IDR.

KET and IBU were used as model BCS class II compounds (poorly soluble, highly permeable). IBU has poor compaction properties and the propensity to stick to tablet presses (40). PAR is used as a model BCS class III compound (highly soluble, poorly permeable) and has reported poor compaction properties (41, 42). A focus variation instrument (Alicona Imaging GmbH, Graz, Austria), which is widely used in micro-precision manufacturing (typically for quality assurance) was used to acquire topographic surface height data in profile (2D) and area (3D) formats along with true colour surface images (43-45). In this study, focus variation microscopy was also utilised to gain insights regarding the surface properties of the drug compacts.

2. Materials and Methods

2.1. Materials

Ketoprofen (KET), Paracetamol (PAR) and Ibuprofen (IBU) were purchased from TCI chemicals (Oxford, UK). Monobasic potassium phosphate and sodium hydroxide were purchased from Sigma Aldrich, UK, and used in the preparation of 0.2 M phosphate buffer at pH 7.2 according to the USP 2019 method (46) for the dissolution experiments.

2.2. Methodology

2.2.1. Preparation of compacts for surface analysis and IDR determinations

Compacts were made using the compact preparation kit (Figure 1) on a computer-controlled M500-50CT instrument with compression plates (Testometric Co. Ltd., UK) A pre-set maximum pressure was set and the compacts for both KET, PAR, and IBU compressed with the displacement accurately measured using a short-travel extensometer at a set speed of 1 mm min^{-1}. KET, PAR and IBU were compacted at 0.25 kN, 0.49 kN, 0.74 kN and 0.98 kN. The

target weight for all compacts was 15 mg with a variation allowance of ± 0.2 mg. One way ANOVA testing ($\alpha = 0.05$) was used to compare the effects of compaction pressure on both IDR and *Sdr* for the four compaction pressures with post hoc *Tukey's* testing applied if significance was reached. Two tailed t-tests ($\alpha = 0.05$) were used to compare the effects of the introduction of the smoother plate insert on IDR and *Sdr* for compacts made at a0.98 kN compression force.

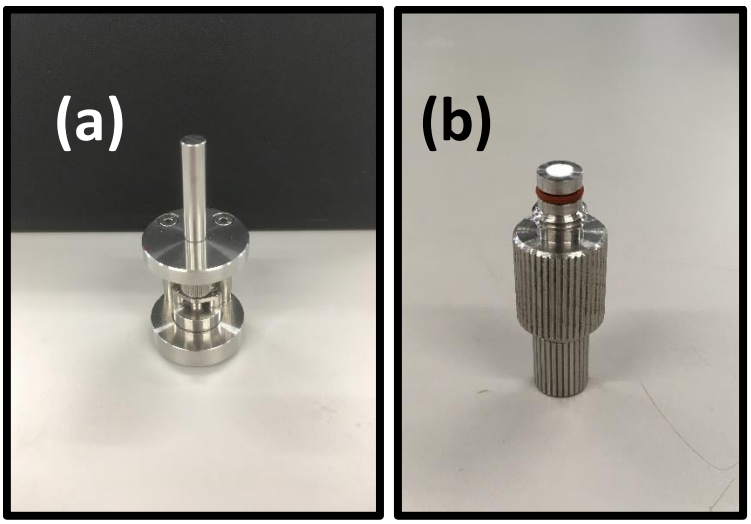

Figure 1. (a)Compact preparation kit, (b) sample compact holder for IDR determination

2.2.2. Tooling effects on the compacts surface analysis

To determine the effect of the tooling on the surface of the compacts and its potential effect on the IDRs, a polished stainless-steel plate was manufactured. SolidWorks® (2018) CAD software was used to design the insert and the rig used for manufacturing the insert. The 3D CAD model and the 2D schematic of the insert and the rig are depicted in Figure 2a and b. The rig in Figure 2b was manufactured from a 316-grade stainless-steel bar. The steel bar was machined on a CNC lathe (Harrison L4 Engineering lathe), and three M3×0.5 holes 20 mm deep were drilled into the rig. The manufactured rig was then chuck mounted and a 50 mm × 50 mm (H × L) mirror-polished stainless-steel grade 316 sheet of 1 mm thickness was inserted

into the rig and excess material was removed to create a circular insert. Before the sheet was inserted into the rig, three holes of diameter 3.4 mm were drilled into the sheet such that the holes in the rig and sheet were aligned (Figure 2c). After the insert was manufactured, it was assembled to the compact forming tooling (Figure 2d). Upon manufacturing, the plate was inserted as depicted (Figure 2d) and compacts of KET, PAR, and IBU were made as described in section 2.2.1.

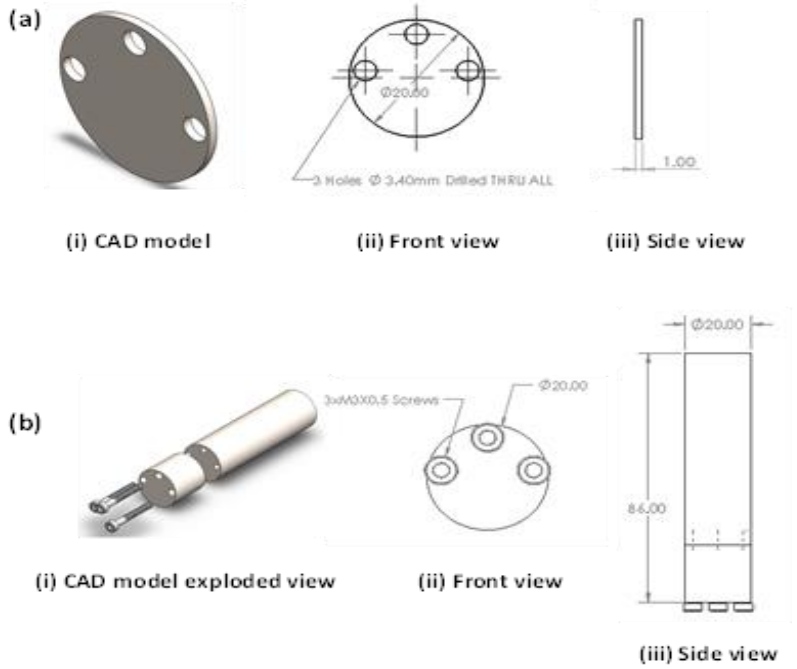

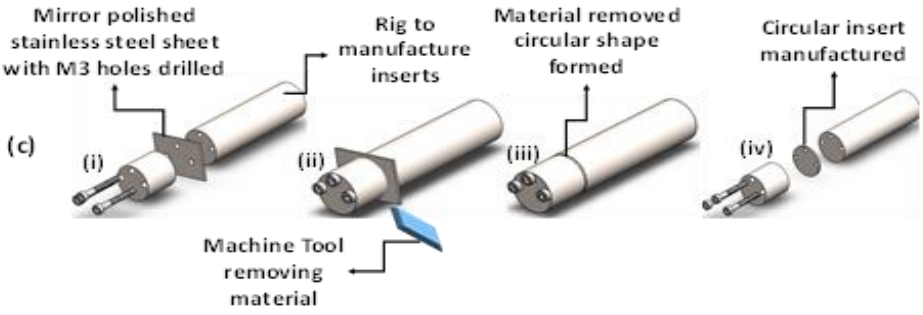

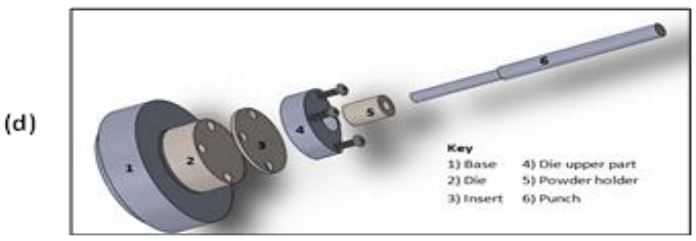

Figure 2. (a) (i) 3D CAD model of an insert, (ii) front view schematic, (ii) side view schematic with general dimensions. All dimensions in mm ± 0.02 mm. (b) (i) 3D CAD model of the rig, (ii) front view schematic, (iii) side view schematic with general dimensions. All dimension in mm ± 0.02 mm. (c) The manufacturing process of a smooth-surfaced insert by using the rig dimensions of the rig in Figure 2b, (i) steel sheet with holes inserted into the rig, (ii) rig closed by M3×0.5 screws and material removed by a machine tool, (iii) rig showing excess material taken off, (iv) rig opened and a circular insert is taken out. (d) A CAD model demonstrating how the insert is assembled with the compact forming tooling.

2.2.3. Surface analysis of tooling and compacts

The surface topography of the original press surface, the developed plate and compacts (3 mm) was analysed using focus variation microscopy (Alicona Infinite Focus microscope, Graz, Austria). Magnifications of 10x and 20x were selected based on previous work by Ward et al. (12). The data from the microscope were processed using the program *Surfstand* (47) providing 3D surface parameters used to characterise the surface topography. Focus variation microscopy relies on different objectives to provide the required sensitivity to resolve the surface. The 20x magnification was selected to achieve the desired vertical resolution of 0.05 µm which was within the recommended microscope operating limits (48). Using the 20x magnification, 16 images of each compact were taken and automatically stitched together to resolve the whole surface with the required detail. Figure 3 shows the process from taking the measurements to data processing. The limitation of this technique to transition between surface textures is described in literature (48). For this reason, the edges of each compact were cropped out as shown in Figure 3. This ensured that erroneous data was not measured from the incidental measurement of the metal rim of the compact. Additionally, images were also cut to the same

size to ensure uniformity in data treatment and to allow comparison of the nature of the drug surfaces.

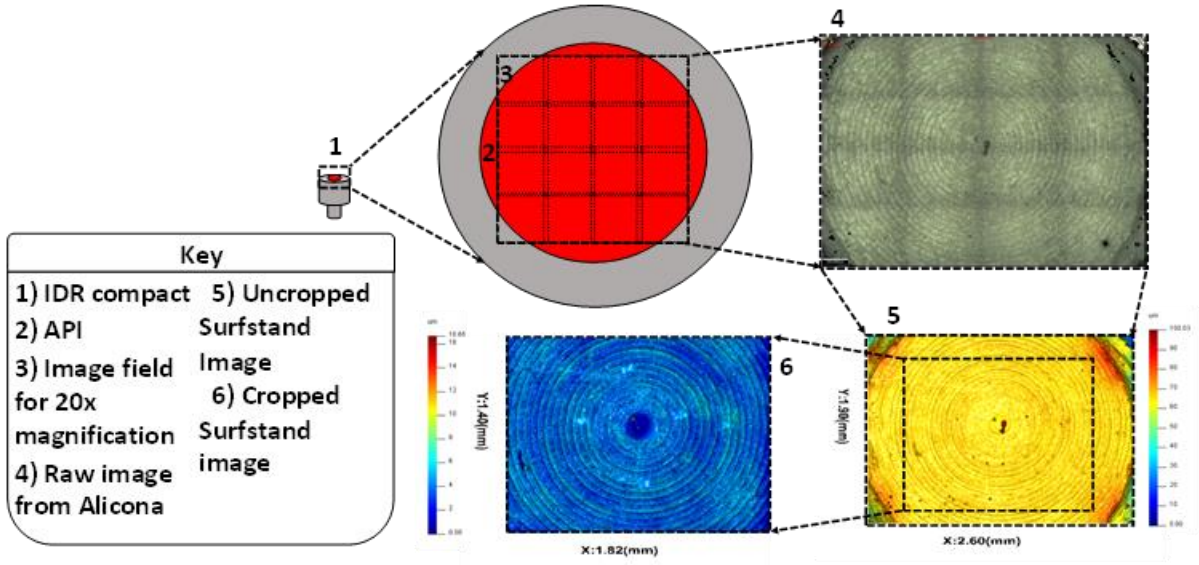

Figure 3. Schematic representation of the measurement zone for the 20x magnification used from which the developed interfacial (surface) area ratio (*Sdr*) was determined.

The *Sdr* parameter, which is the developed interfacial (surface) area ratio (equation 1) allowed the influence of the different compressions on the surface topology of the compacts to be evaluated. *Sdr* is defined as the surface area gain of the textured sample surfaces compared to that of its cross-sectional area. By doing this comparison of textured surface area gain, the parameter *Sdr* is always expressed as a percentage where the cross-sectional area of a surface is zero percent and any texture to this same surface will increase the Sdr percentage, relative to that of the cross-sectional area. This allows for the surface gain (surface area) to be calculated meaning that differences between the compacts made from the original press surface and the developed plate can be ascertained. The same compacts used for the *Sdr* measurements were used for IDR determinations. Along with the *Sdr* data, 23 other surface parameters were also generated for each compact surface. Although, some of these other surface parameters were

shown to be of some use in the analysis of drug compacts (49), this study focused solely on the *Sdr* parameter with the aim of showing a direct relationship between surface gain and IDR determination performance.

$$Sdr = \frac{(Texture\ Surface\ Area) - (Cross\ Sectional\ Area)}{Cross\ Sectional\ Area} * 100 \qquad \text{Equation 1}$$

2.2.4. Dissolution imaging

The SDI2 compact flow cell (Figure 4a) was used for the IDR determinations. Each dissolution experiment lasted 21 min (including 1 min period where a higher flow rate of 5 mL/min was applied to fill the compact flow cell). This was implemented to flush away loose particles on the surface. A flow rate of 2.0 mL/min was applied for the following 20 min. The experiments were conducted in phosphate buffer (pH 7.2) at 37 ˚C. Dissolution imaging was conducted at the wavelengths 255 nm (UV) and 520 nm (Vis). All experiments were conducted 5 times (n=5).

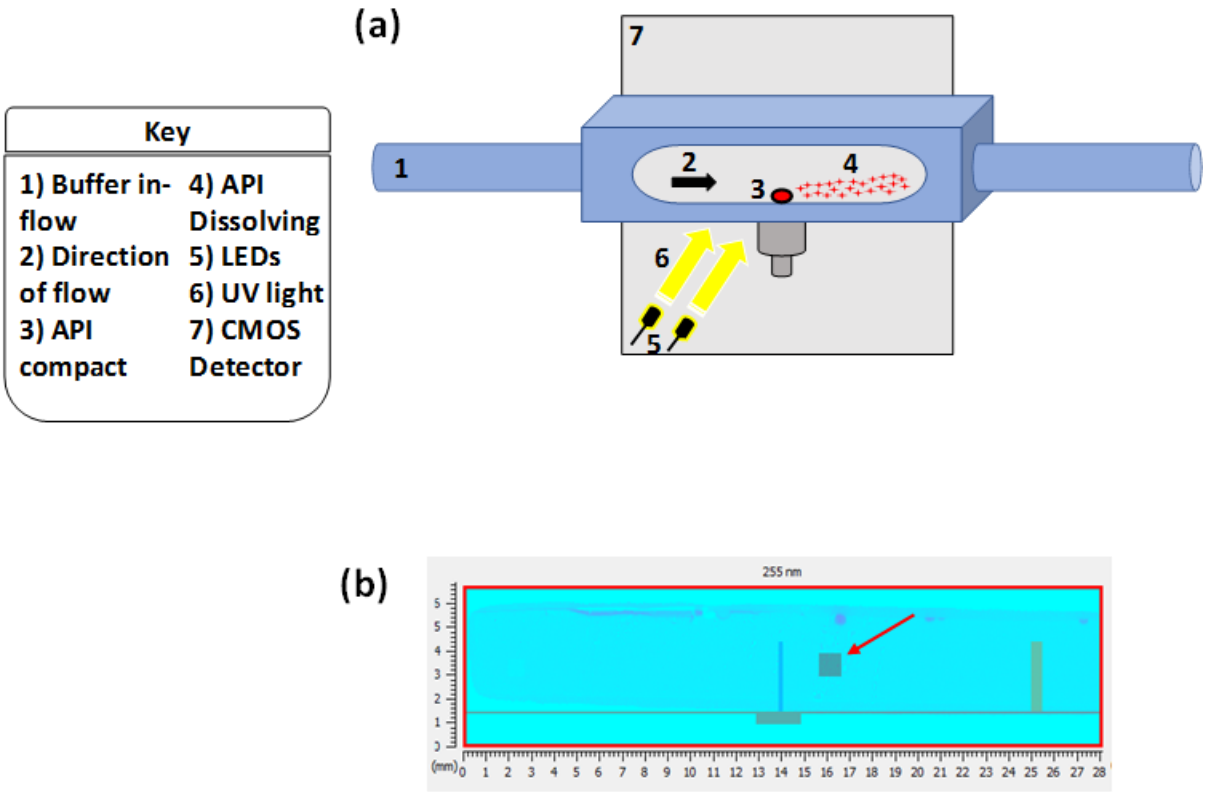

198

199 Figure 4. (a) Schematic representation of a compact flow-through cell for the SDI2 system for
200 IDR determinations (b) 1 cm x 1 cm box used in the data collection for the calibration of either
201 KET, PAR or IBU for molar extinction coefficient determinations

202

203 Analysis of the dissolution images was performed using the SDI2 software (Pion Inc., version
204 3.0.22). The molar extinction coefficients for the drugs were experimentally determined over
205 seven concentration levels (KET 2 µg/mL - 18 µg/mL, PAR 10 µg/mL - 80 µg/mL and IBU 25
206 µg/mL – 500 µg/mL) in the phosphate buffer (pH 7.2). Calibration curves were derived from
207 two stocks solutions and conducted in triplicate and had r^2 values ranging from 0.9919 – 0.9966
208 (all calibration curves were within the linear range). A 1 cm by 1 cm box was set to collect
209 absorbance values and placed in the middle of the cell (red arrow on Figure 4b). Absorbance
210 data for the calibration curve were collected at 30 s intervals over the last 5 min of each 10 min
211 run of the standards. Intrinsic dissolution rates were calculated by incorporating the molar

extinction coefficient (MEC) of each drug into the provided software (Pion Inc., version 3.0.22).

2.2.5. X-ray powder diffraction (XRPD)

The XRPD patterns were determined for the bulk powders of KET, IBU and PAR. XRPD patterns were also determined after the compaction process (powder was removed from the compact disc and analysed) and after the 21 min long IDR experiment (powder was removed after drying in an oven at 40 °C for an hour and analysed) for compacts made at a compaction force of 0.98 kN. This allowed for the influence of the compression and dissolution process on the solid-state properties of the compacts to be assessed. All compacts were scanned in Bragg–Brentano geometry, over a scattering (Bragg, 2θ) angle range from 5 to 100°, in 0.02° steps at 1.5° min^{-1} using a D2 Phaser diffractometer (Bruker AXS GmbH, Karlsruhe, Germany) (50). Microsoft Excel was used to analyse the collected XRPD patterns.

3. RESULTS AND DISCUSSION

3.1. Impact of tooling on the surface topography of the compacts

The quality of compacts and their surfaces may affect drug dissolution behaviour. Andersson et al. reported that the quality of the disc during disc dissolution affected the variability of IDR values using the µDISS (9). The focus variation instrument provides quantitative data that allows for the topology of surfaces to be investigated. Figure 5a and 5b depict the images of the surfaces of the original press surface and the manufactured steel plate insert, respectively.

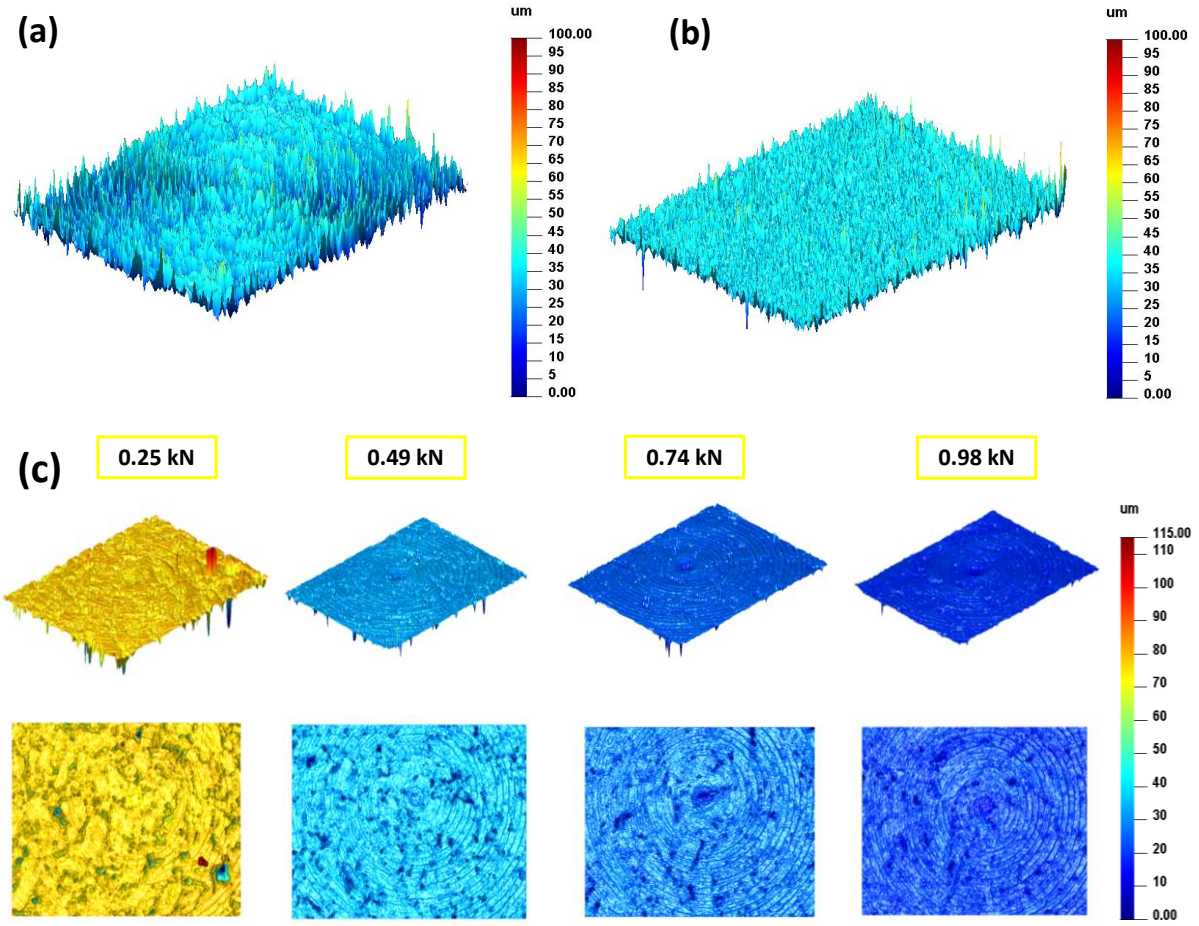

Figure 5. 3D images of the roughness of the original (a), and the manufactured plate insert surfaces (b), both used in the production compacts for IDR determinations. 3D images of the surfaces of IBU compacts at varying compressions of forces using the original press surface (c)

The images highlight the differences with respect to the roughness of the surfaces, which may affect the surfaces of the compacts produced. The manufactured plate insert had a significantly lower *Sdr* (8.6 %) as compared to that of the original press surface (19.9 %). The IBU compacts (from the original press surface) show visually that an increase in the compression force of the compacts brought about a decrease in the compact surface roughness (Figure 5c). This was also evident from Table 1, where generally, the higher the compression force, the lower the *Sdr* value of the compact. One way-ANOVA testing showed that the changes in compaction force had a significant effect on the *Sdr* with PAR and IBU ($p < 0.05$) but not for KET ($p > 0.05$).

However, a *Tukey's* post hoc test of PAR failed to identify any trend in the *Sdr* data indicating that there was not a strong correlation between compaction force and the surface roughness of the PAR compacts. These findings may be due to the elastic nature of PAR (40, 41). Post hoc *Tukey's* testing with IBU showed that higher compaction forces resulted in a lower *Sdr*. In respect to *Sdr* no distinction between 0.98 kN and 0.74 kN could be made. However, statistical testing showed that the 0.98 kN and 0.74 kN compaction forces resulted in a lower *Sdr* when compared to 0.49 kN and that all compaction forces were gave a lower *Sdr* when compared to the 0.25 kN.

Table 1. Developed interfacial (surface) area ratio (*Sdr*) for KET, PAR and IBU 3 mm compacts from the different compaction forces and the manufactured plate insert (at 0.98 kN plate). All experiments were conducted 5 times (n=5) and reported with their standard deviations.

	Ketoprofen (KET)	Paracetamol (PAR)	Ibuprofen (IBU)
Compact	*Sdr* (%)	*Sdr* (%)	*Sdr* (%)
0.25 kN	3.3 ± 3.6	5.0 ± 1.1	8.3 ± 1.1
0.49 kN	0.6 ± 0.4	7.6 ± 2.1	3.2 ± 0.6
0.74 kN	0.3 ± 0.1	7.2 ± 2.9	1.4 ± 0.2
0.98 kN	0.3 ± 0.0	3.9 ± 1.6	0.6 ± 0.2
0.98 kN plate	0.1 ± 0.0	17.9 ± 12.7	0.8 ± 0.5

Figure 6 depicts the images of compact surfaces obtained from the compaction force at 0.98 kN for the original press surface and the manufactured plate insert using the focus variation microscope. With the introduction of the plate insert, KET showed a reduction in *Sdr* from 0.3 % (original press surface) to 0.1 % (manufactured plate insert) (Figure 6a and Table 1). This was very close to a theoretical flat plane of 0 %. These surfaces were shown to be statistically different ($p < 0.05$).

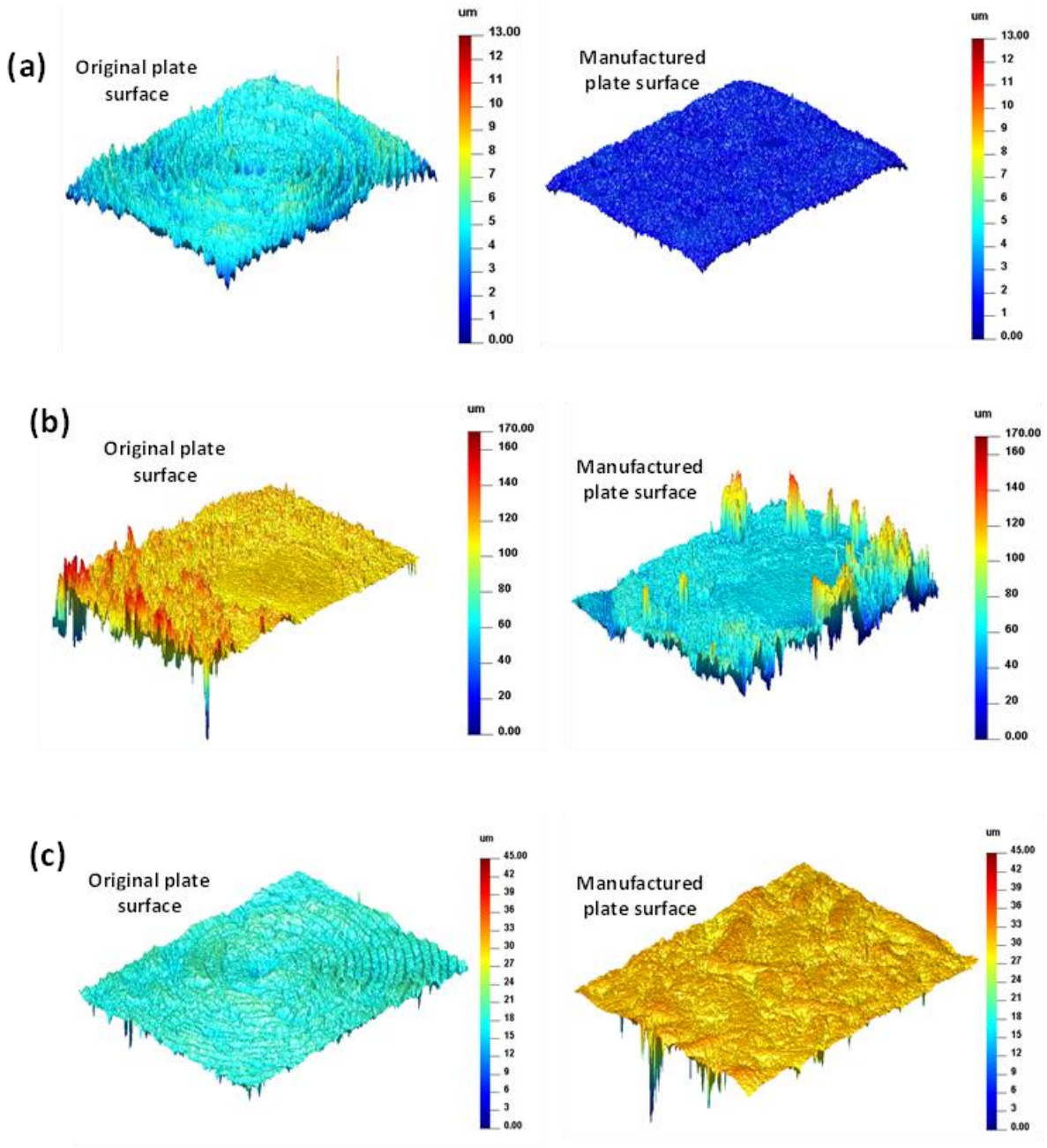

Figure 6. 3D images of the surface roughness from the focus variation instrument for (a) KET, (b) PAR (c) IBU compacts at 0.98 kN using the original press surface and the manufactured plate insert also at 0.98 kN.

Using the compaction pressure of 0.98 kN, the manufactured plate insert caused an increase in the *Sdr* values for PAR and IBU (Figure 6b and c, Table 1). For PAR especially, there was a large increase in the mean *Sdr* value (3.9 %) to (17.9 %). These differences in the *Sdr* for PAR

and IBU were however not statistically significant. This may be due to the higher standard deviations experienced by the PAR and IBU compacts thereby indicating a decrease in repeatability. This is evident in the individual images (n = 5 images) obtained from the focus variation instrument (images not included).

XRPD (supplementary material) showed that the PAR used was form I. This form tends to have poor compaction properties resulting from a crystal structure of corrugated hydrogen-bonded layers, which lack the ability to stack flat (37, 38). It would seem, in the case of PAR and IBU, that the ring like pattern from the original press surface may be preferable, as the added texture provides a surface that is less prone to sticking. The relatively smoother inserted plate seems to be of no or very limited benefit to such APIs and therefore care and consideration should as such be given to the nature of API during the compact preparation process.

3.2. Intrinsic dissolution rate determinations

Figure 7a, 8a and 9a depict the UV images for the IDR determinations of KET, PAR and IBU respectively. The images for each compaction force were seen to be very similar. This correlated well to similar IDR values for each of the APIs over the course of the experiments. In the dissolution studies (at every test condition), the IDR of the drug substances had reached a plateau by 5 min. The blue, red and yellow inserts in Figure 7 - 9c for KET, PAR and IBU, respectively, showed increased variability prior to the 5 min mark. This high IDR variability from the 0 – 5 min mark may have been attributed to the dissolution of residual/loose drug particles on the surface of the compacts. The initial high IDR variability phase has also been the region in which fractal-like dissolution as described by Niderquell and Kuentz has been observed (20). This phenomenon may be caused by differences in crystal morphology or the particle size of drug on the compact surface (20). This was particularly prominent for KET

(Figure 7b, 7c). IDR values for both PAR and IBU reached a plateau quicker as seen in Figure 8b, 8c, and Figure 9b, 9c respectively.

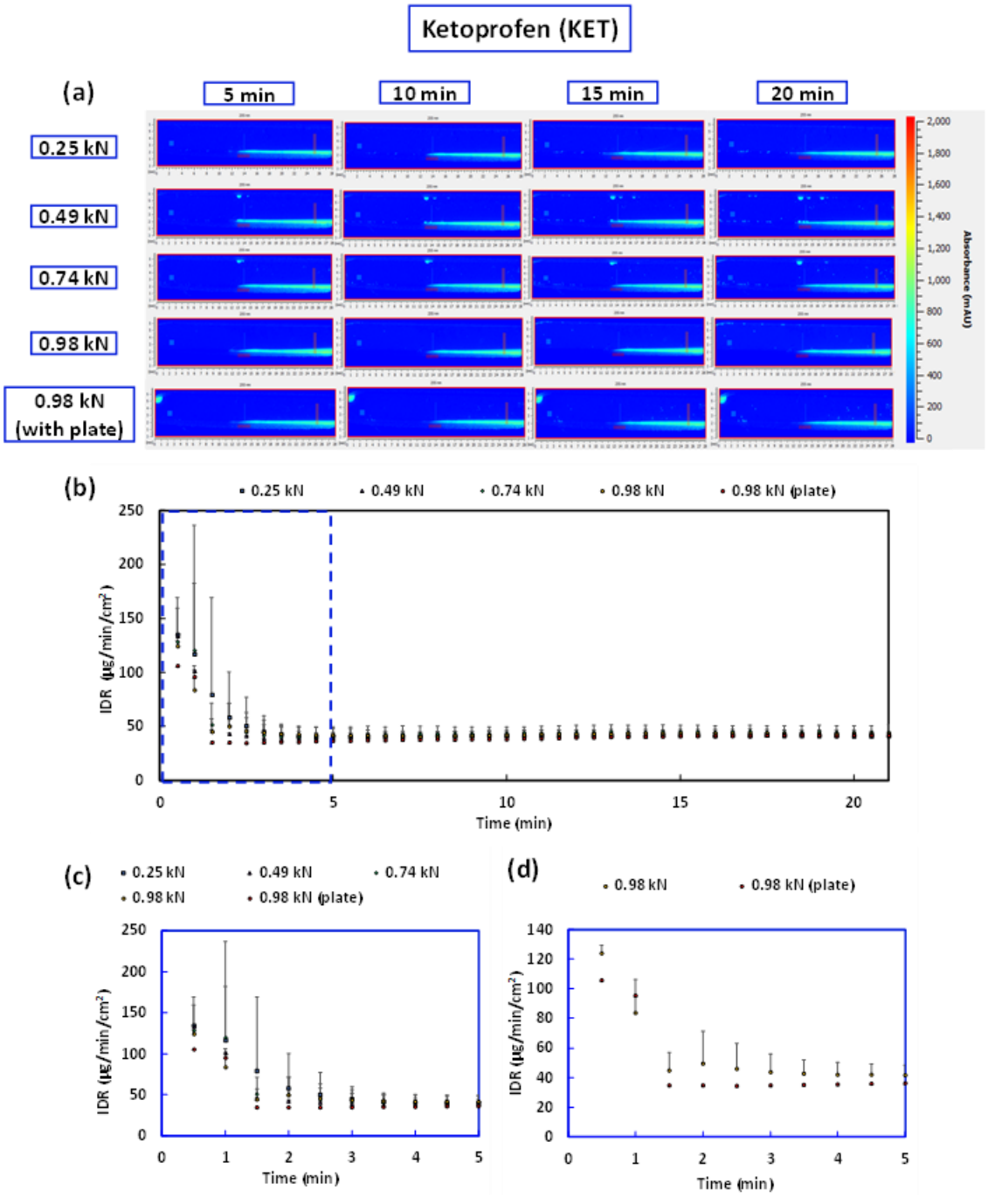

Figure 7. (a) Surface dissolution imaging of KET at 0.25, 0. 49, 0.74, 0.98 and 0.98 kN (with manufactured plate) at 5, 10, 15 and 20 min time points. (b) IDR as a function of time for of KET at 0.25, 0. 49, 0.74, 0.98 and 0.98 kN (with manufactured plate). Blue insert in figure 7b is to elaborate this point hence why IDR was reported after the 5 min mark only. The zoom-in

of the blue insert is depicted as figure 7c for clarity. Figure 8d compares the compacts at 0.98 kN with and without the plate insert to show the significant reduction in variability as a result.

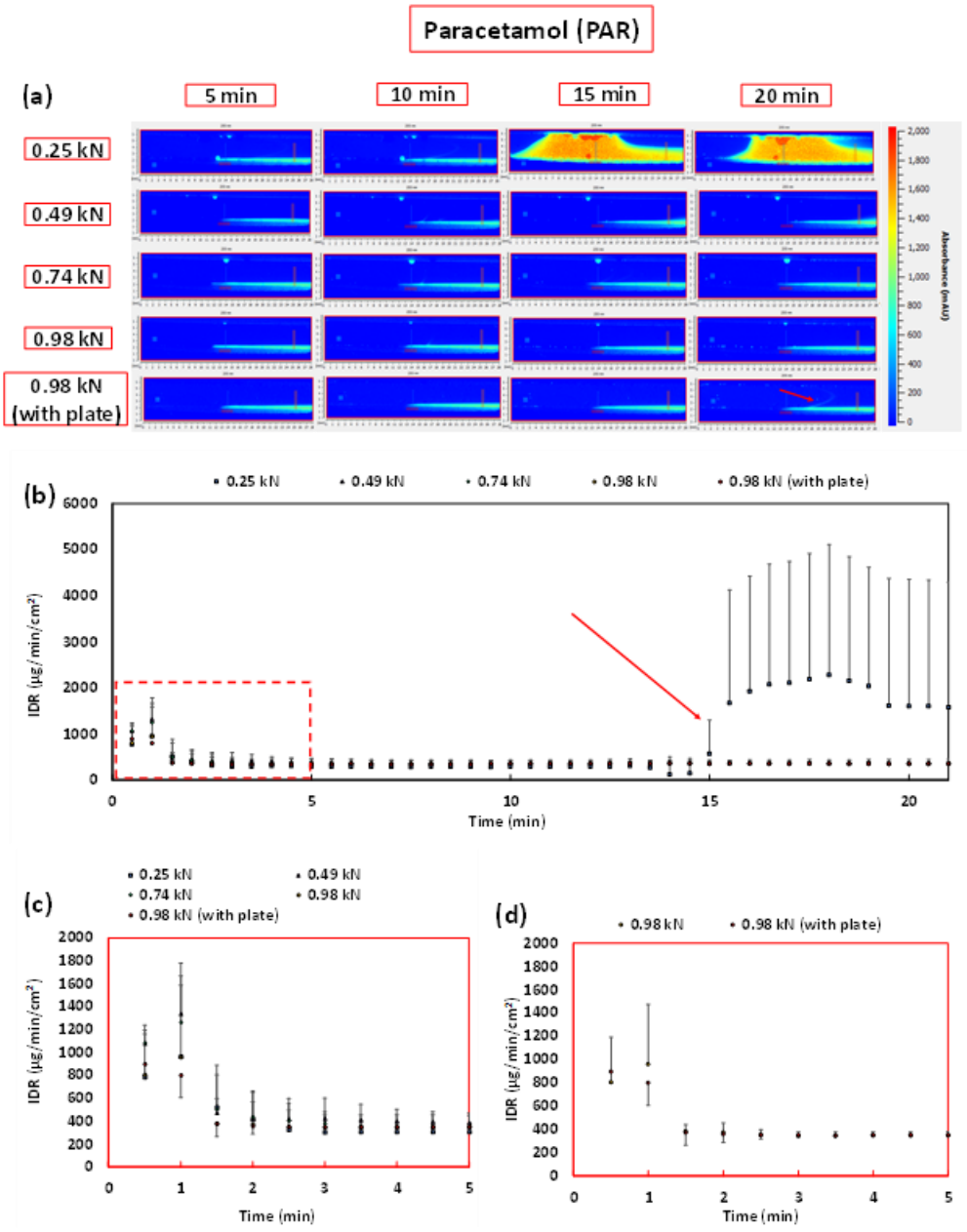

Figure 8. (a) Surface dissolution imaging of PAR at 0.25, 0. 49, 0.74, 0.98 and 0.98 kN (with manufactured plate) at 5, 10, 15 and 20 min time points. (b) IDR as a function of time for of PAR at 0.25, 0. 49, 0.74, 0.98 and 0.98 kN (with manufactured plate). The red insert in figure 8b is to elaborate this point hence why IDR was reported after the 5 min mark only. The 0.25 kN compact failure is indicated by the red arrow. The zoom-in of the red insert is depicted as

311 Figure 8c for clarity. Figure 8d compares the compacts at 0.98 kN with and without the plate
312 insert to show the significant reduction in variability as a result.

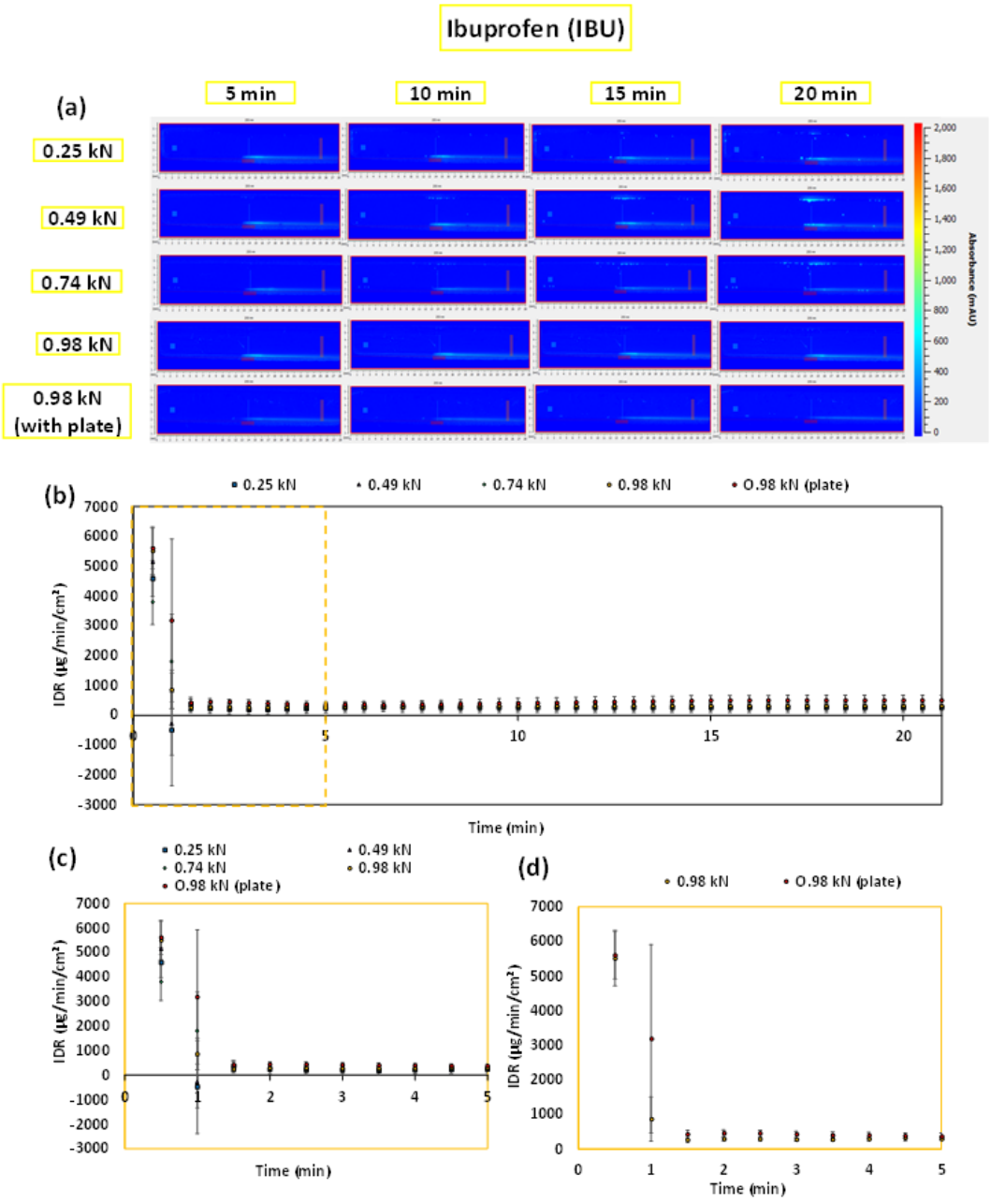

313

314 Figure 9. (a) Surface dissolution imaging of IBU at 0.25, 0. 49, 0.74, 0.98 and 0.98 kN (with
315 manufactured plate) at 5, 10, 15 and 20 min time points. (b) IDR as a function of time for of
316 IBU at 0.25, 0. 49, 0.74, 0.98 and 0.98 kN (with manufactured plate). The zoom-in of the
317 yellow insert is depicted as Figure 9c for clarity. Figure 9d compares the compacts at 0.98 kN
318 with and without the plate insert to show the significant reduction in variability as a result.

Although most images for all IDR determinations looked similar, differences can be found with the PAR 0.25 kN after the 15 min time point. Large amounts of PAR were seen in the dissolution stream in the image field. This inflated the average IDR value from 339 µg/min/cm^2 (pre 15 min) to 1814 µg/min/cm^2 (post 15 min). This was also be visualised in Figure 8b (indicated by the red arrow) where the increase in the absorbance lead to a significant increase in the IDR value of PAR. Upon further inspection of the images and the compact post dissolution, it appeared a complete breakdown of the compact had occurred. This suggested a compaction force of 0.25 kN was too low for PAR. Additionally a "wave" (red arrow on Figure 8a) was also be seen in the UV image for the 0.98 kN compact (with the manufactured plate insert). This wave formation may have been PAR particulates dissolving faster into the dissolution stream from the compact.

Table 2 depicts the average IDR values of the API's post 5 min. The data did not exhibit a trend in IDR values ($p > 0.05$) or their standard deviations with respect to compaction force changes. This was consistent with work by Alsenz et al. where a range of compaction forces from 0.07 kN to 0.2 kN used to compact 4 mg micro discs of KET for miniaturised IDR determination did not demonstrate any significant effects on the IDR (13). Löbmann et al. did not show any significant correlation between IDR and compaction pressure using crystalline indomethacin, however this was not the case for the amorphous form (25). This indicates that any correlation between IDR performance and compaction force may be form dependent.

Table 2. Intrinsic dissolution rates (IDR) for KET, PAR and IBU 3 mm compacts from the different compaction forces and a manufactured plate insert. All experiments were conducted 5 times (n=5) and reported with their standard deviations.

	Ketoprofen (KET)	Paracetamol (PAR)	Ibuprofen (IBU)
Compact	IDR (µg/min/cm²)	IDR (µg/min/cm²)	IDR (µg/min/cm²)
0.25 kN	41 ± 3	1078 ± 1162	263 ± 168

0.49 kN	42 ± 1	375 ± 48	296 ± 79
0.74 kN	44 ± 7	355 ± 26	279 ± 62
0.98 kN	42 ± 4	364 ± 32	314 ± 49
0.98 kN plate	39 ± 3	357 ± 18	452 ± 146

341

342 The introduction of the manufactured plate had little effect on the IDR determinations. The
343 recorded changes in the IDR values were not statistically significant. This suggests that the use
344 of the manufactured plate insert did not improve IDR determination or that the inferior surface
345 properties actually spilled over to variation with respect to dissolution behaviour. This is also
346 evident on Figure 6c where the manufactured plate insert increased the surface roughness of
347 the IBU compacts thereby increasing the surface heterogeneity.

348 For all test conditions, the relative standard deviation (expressed here as a percentage for
349 comparison purposes) of the IDR value varied between 1 - 13 % (average 7 %) for KET, 5 –
350 96 % (average 25 %) for PAR and 14 – 57 % (average 33 %) for IBU. The apparent larger
351 variation in the PAR IDR determination is largely skewed by the inflated IDR determination
352 for the 0.25 kN experiments. Similar levels of variation have been reported using the Sirius
353 SDI dissolution imaging system, a predecessor of the instrument applied in the current study
354 (10), and the μDISS Profiler™ (9). Etherson et al reported in an inter-laboratory small-scale
355 dissolution study that the relative standard deviation (expressed as a percentage) of IDR values
356 varied from 33-130 % using 6 compounds (n = 6), and FaSSIF and blank FaSSIF as the
357 dissolution media across seven sites (10). For IBU, there was a large variation in the absolute
358 measured IDR values from the two generation of the SDI equipment. Etherson et al using the
359 first generation recorded an IDR for IBU of 66 μg/min/cm^2 (n = 6), using blank FaSSIF version
360 1 (46), whereas this study using the second generation reports an IBU IDR of 320 μg/min/cm^2
361 using phosphate buffer, pH 7.2, as the dissolution media. This vast difference in absolute IDR
362 values between the first generation (SDI) and second generation (SDI2), may be attributed to

the different media used, however it is also highly likely that experimental set-up and data processing had an impact. Using the μDISS Profiler™, Andersson et al. also found IDR measurements with similar levels of relative standard deviation (35 – 127 %, expressed as a percentage for comparison purposes), with 6 compounds (n = 3), using FaSSIF and phosphate buffer pH 6.5 as the dissolution media. This would indicate that each of these small-scale IDR determination methods give similar levels of variations.

XRPD (supplementary Figures S1-S3) showed that polymorphic changes did not occur during the compaction and IDR determination process. The XRPD distinctive peaks for KET, IBU and PAR are published elsewhere (14, 37, 40, 51, 52).

4. Conclusion

This study demonstrated that surface characteristics of drug compacts can be successfully studied using focus variation microscopy. In general, higher compaction forces resulted in smoother compacts, although statistically significant differences were only reached for IBU, which suggests this relationship may be API dependent. For KET, the use of a relatively smooth manufactured plate insert produced a smoother compact as measured by a reduction in the *Sdr* value. The opposite was true for PAR and IBU compacts, which is most likely as a result of the poor compaction properties associated with these compounds This suggests that the ability of a smooth compaction surface to produce a smooth compact is also API dependent. Despite the differences in drug compact surfaces with changes in compaction force and changes in the compaction surface, statistical differences were not shown in the IDR measurements. The variation associated with measuring IDR using the SDI2, appears to be comparable to that of the other small-scale IDR determination methods. This study thus highlights the ability of the focus variation instrument to provide a quantitative way to analyse drug compacts surfaces prior to IDR determination.

5. Acknowledgements

The authors acknowledge the EPSRC DTP at the University of Huddersfield for financial support for Benedict Brown. The authors also acknowledge Becky Upton and Breeze Outwaite (formerly of Pion, UK), Hayley Watson and Karl Box of Pion, UK for their technical expertise on the use of the SDI2 instrument. The authors also thank Charlotte Ayres and Professor Jonathan Steed of the University of Durham for their assistance.

Author Contributions

Benedict Brown: Data curation; Formal analysis; Methodology; Investigation, Writing—Original Draft; Writing—Review & Editing. Zayeem Fazili: Data curation; Formal analysis; Methodology; Investigation, Writing—Original Draft; Adam Ward: Data curation; Formal analysis; Methodology; Investigation. Karl Walton: Conceptualisation; Supervision; Data curation. Liam Blunt: Conceptualisation; Supervision. Jesper Østergaard: Methodology; Investigation; Writing—Review & Editing. Kofi Asare-Addo: Conceptualisation; Supervision; Writing—Original Draft; Writing—Review & Editing;

Conflicts of Interest

The authors declare no conflict of interest.

Supplementary materials

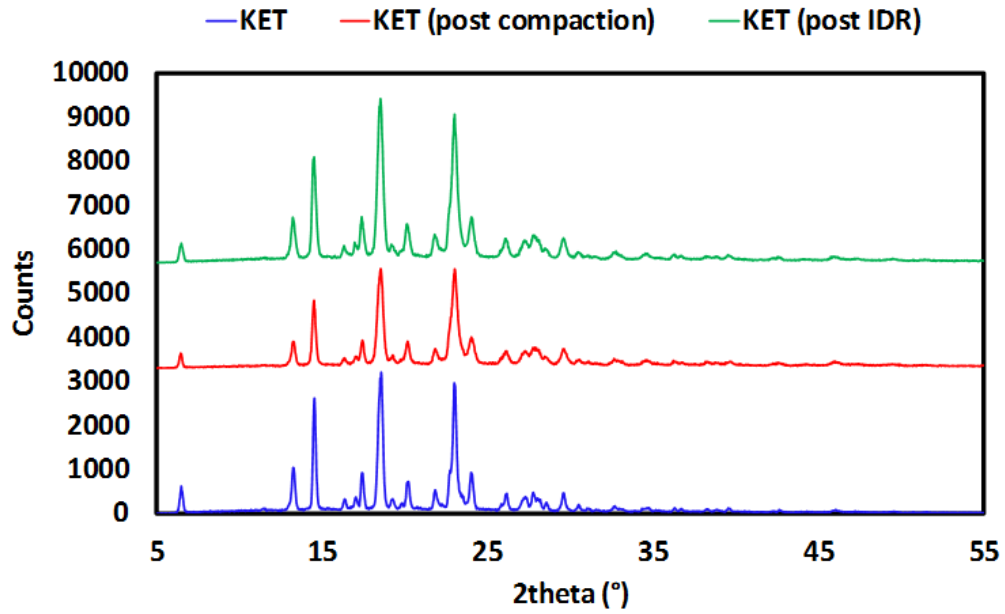

407

408 Figure S1. XRPD analysis for KET (powder as received), KET (post compaction) and KET
409 (post IDR run) demonstrating no changes.

410

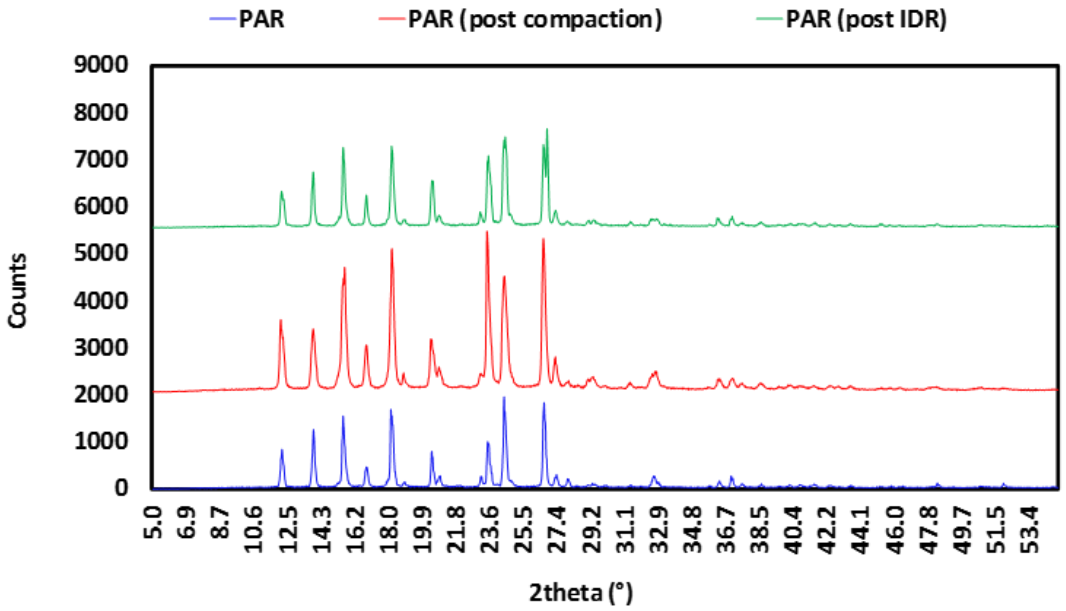

411

412 Figure S2. XRPD analysis for PAR (powder as received), PAR (post compaction) and PAR

413 (post IDR run) demonstrating no changes.

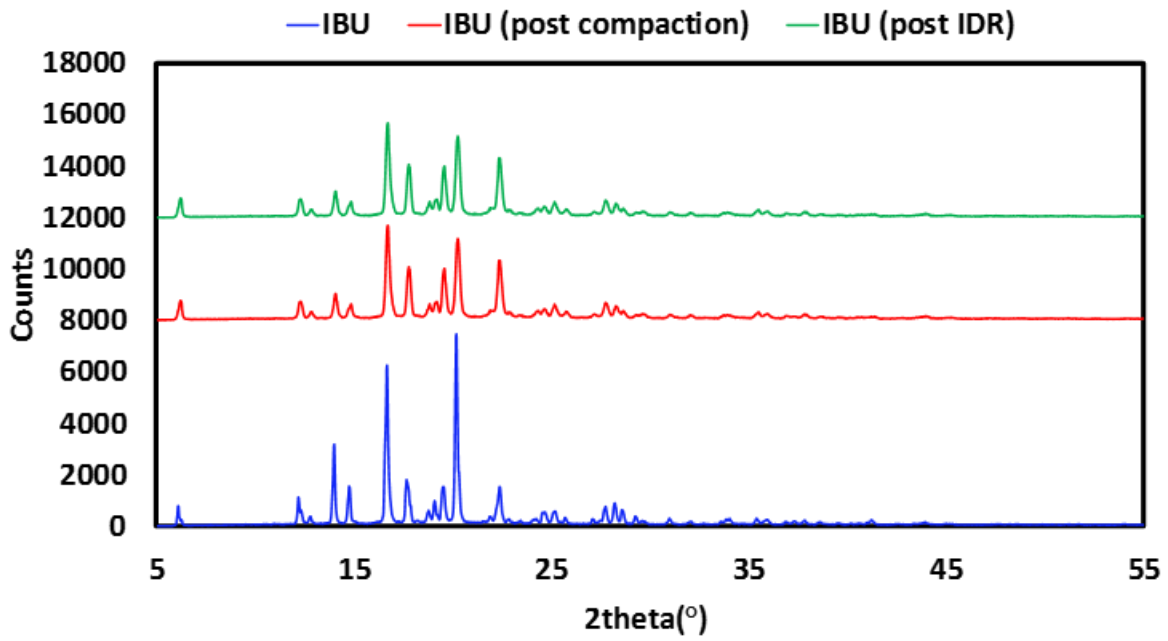

414

415 Figure S3. XRPD analysis for IBU (powder as received), IBU (post compaction) and IBU

416 (post IDR run) demonstrating no changes.

417

418

419

420

421

422

423

424

425

426

427

6. References

1. Amidon GL, Lennernäs H, Shah VP, Crison JR. A theoretical basis for a biopharmaceutic drug classification: the correlation of in vitro drug product dissolution and in vivo bioavailability. Pharmaceutical research. 1995;12(3):413-420.
2. Kanikkannan, N. (2018). Technologies to improve the solubility, dissolution and bioavailability of poorly soluble drugs. *J Anal Pharm Res*, *7*(1), 00198.
3. Bergström CAS, Andersson SBE, Fagerberg JH, Ragnarsson G, Lindahl A,. Is the full potential of the biopharmaceutics classification system reached? European Journal of Pharmaceutical Sciences. 2014;57(1):224-231.
4. Butler JM, Dressman JB. The developability classification system: application of biopharmaceutics concepts to formulation development. Journal of pharmaceutical sciences. 2010;99(12):4940-4954.
5. Bergström, C. A., Box, K., Holm, R., Matthews, W., McAllister, M., Müllertz, A., ... & Teleki, A. (2019). Biorelevant intrinsic dissolution profiling in early drug development: Fundamental, methodological, and industrial aspects. *European Journal of Pharmaceutics and Biopharmaceutics*, *139*, 101-114.6.
6. Mauger J, Ballard J, Brockson R, De S, Gray V, Robinson D. Intrinsic dissolution performance testing of the USP dissolution apparatus 2 (Rotating Paddle) Using modified salicylic acid calibrator tablets: Proof of principle. Dissolution Technologies. 2003;10(3):6-15.
7. Hulse WL, Gray J, Forbes RT. A discriminatory intrinsic dissolution study using UV area imaging analysis to gain additional insights into the dissolution behaviour of active pharmaceutical ingredients. International Journal of Pharmaceutics. 2012;434(1-2):133-139.
8. Yu LX, Carlin AS, Amidon GL, Hussain AS. Feasibility studies of utilizing disk intrinsic dissolution rate to classify drugs. International Journal of Pharmaceutics. 2004;270(1):221-227.
9. Andersson SB, Alvebratt C, Bevernage J, Bonneau D, da Costa Mathews C, Dattani R, Edueng K, He Y, Holm R, Madsen C. Interlaboratory validation of small-scale solubility and dissolution measurements of poorly water-soluble drugs. Journal of pharmaceutical sciences. 2016;105(9):2864-2872.
10. Etherson, K., Dunn, C., Matthews, W., Pamelund, H., Barragat, C., Sanderson, N., Izumi, T., da Costa Mathews, C., Halbert, G., Wilson, C. and McAllister, M., 2020. An interlaboratory investigation of intrinsic dissolution rate determination using surface dissolution. *European Journal of Pharmaceutics and Biopharmaceutics*, *150*, pp.24-32.
11. Kuentz M. Analytical technologies for real-time drug dissolution and precipitation testing on a small scale. Journal of Pharmacy and Pharmacology. 2015;67(2):143-159.
12. Macheras P, Dokoumetzidis A. On the Heterogeneity of Drug Dissolution and Release. Pharmaceutical Research. 2000;17(2):108-112.

13. Alsenz J, Haenel E, Anedda A, Du Castel P, Cirelli G. Miniaturized INtrinsic DISsolution Screening (MINDISS) assay for preformulation. Eur J Pharm Sci. 2016;87:3-13.

14. Ward A, Walton K, Box K, Østergaard J, Gillie LJ, Conway BR, Asare-Addo K. Variable-focus microscopy and UV surface dissolution imaging as complementary techniques in intrinsic dissolution rate determination. International Journal of Pharmaceutics. 2017;530(1-2):139-144.

15. Avdeef A, Tsinman O. Miniaturized rotating disk intrinsic dissolution rate measurement: Effects of buffer capacity in comparisons to traditional wood's apparatus. Pharmaceutical Research. 2008;25(11):2613-2627.

16. Berger CM, Tsinman O, Voloboy D, Lipp D, Stones S, Avdeef A. Technical note: Miniaturized intrinsic dissolution rate (Mini-IDR™) measurement of griseofulvin and carbamazepine. Dissolution Technologies. 2007;14(4):39-41.

17. Alsenz J ME, Haenel E. Development of a partially automated solubility screening (PASS) assay for early drug development. Journal of pharmaceutical sciences. 2007;96(7).

18. Wyttenbach N, Alsenz J, Grassmann O. Miniaturized Assay for Solubility and Residual Solid Screening (SORESOS) in Early Drug Development. Pharmaceutical Research. 2007;24(5):888-898.

19. Long CM, Tang K, Chokshi H, Fotaki N. Surface Dissolution UV Imaging for Investigation of Dissolution of Poorly Soluble Drugs and Their Amorphous Formulation. AAPS PharmSciTech. 2019;20(3):1-12.

20. Niederquell A, Kuentz M. Biorelevant dissolution of poorly soluble weak acids studied by UV imaging reveals ranges of fractal-like kinetics. International Journal of Pharmaceutics. 2014;463(1):38-49.

21. Boetker JP, Savolainen M, Koradia V, Tian F, Rades T, Müllertz A, Cornett C, Rantanen J, Østergaard J. Insights into the Early Dissolution Events of Amlodipine Using UV Imaging and Raman Spectroscopy. Molecular Pharmaceutics. 2011;8(4):1372-1380.

22. Gordon S, Naelapää K, Rantanen J, Selen A, Müllertz A, Østergaard J. Real-time dissolution behavior of furosemide in biorelevant media as determined by UV imaging. Pharmaceutical Development and Technology. 2013;18(6):1407-1416.

23. Qiao N, Wang K, Schlindwein W, Davies A, Li M. In situ monitoring of carbamazepine–nicotinamide cocrystal intrinsic dissolution behaviour. European Journal of Pharmaceutics and Biopharmaceutics. 2013;83(3):415-426.

24. Lu Y, Li M. Simultaneous rapid determination of the solubility and diffusion coefficients of a poorly water-soluble drug based on a novel UV imaging system. Journal of pharmaceutical sciences. 2016;105(1):131-138.

25. Löbmann K, Flouda K, Qiu D, Tsolakou T, Wang W, Rades T. The influence of pressure on the intrinsic dissolution rate of amorphous indomethacin. Pharmaceutics. 2014 Sep;6(3):481-93.

26. Colombo S, Brisander M, Haglöf J, Sjövall P, Andersson P, Østergaard J, Malmsten M, Medicinteknik. Matrix effects in nilotinib formulations with pH-responsive polymer

produced by carbon dioxide-mediated precipitation. International Journal of Pharmaceutics. 2015;494(1):205-217.

27. Ye F, Yaghmur A, Jensen H, Larsen SW, Larsen C, Østergaard J. Real-time UV imaging of drug diffusion and release from Pluronic F127 hydrogels. European Journal of Pharmaceutical Sciences. 2011;43(4):236-243.

28. Østergaard J, Meng-Lund E, Larsen SW, Larsen C, Petersson K, Lenke J, Jensen H. Real-Time UV Imaging of Nicotine Release from Transdermal Patch. Pharmaceutical Research. 2010;27(12):2614-2623.

29. Østergaard J, Wu JX, Naelapää K, Boetker JP, Jensen H, Rantanen J. Simultaneous UV imaging and Raman spectroscopy for the measurement of solvent-mediated phase transformations during dissolution testing. Journal of pharmaceutical sciences. 2014;103(4):1149-1156.

30. Boetker JP, Rantanen J, Rades T, Müllertz A, Østergaard J, Jensen H. A New Approach to Dissolution Testing by UV Imaging and Finite Element Simulations. Pharmaceutical Research. 2013;30(5):1328-1337.

31. Østergaard J. UV imaging in pharmaceutical analysis. Journal of Pharmaceutical and Biomedical Analysis. 2018;147:140-148.

32. Ward, A., Walton, K., Stoycheva, S., Wallis, M., Adebisi, A., Nep, E., Ngwuluka, N.C., Shaboun, S., Smith, A.M., Conway, B.R. and Asare-Addo, K., 2020. The use of visible and UV dissolution imaging for the assessment of propranolol hydrochloride in liquisolid compacts of Sesamum radiatum gum. *Journal of Drug Delivery Science and Technology*, p.101511.

33. Sun Y, Chapman A, Larsen SW, Jensen H, Petersen NJ, Goodall DM, Østergaard J. UV–vis Imaging of Piroxicam Supersaturation, Precipitation, and Dissolution in a Flow-Through Setup. Analytical Chemistry. 2018;90(11):6413-6418.

34. Asare-Addo K, Walton K, Ward A, Totea A-M, Taheri S, Alshafiee M, Mawla N, Bondi A, Evans W, Adebisi A, Conway BR, Timmins P. Direct imaging of the dissolution of salt forms of a carboxylic acid drug. International Journal of Pharmaceutics. 2018;551(1-2):290-299.

35. Asare-Addo K, Alshafiee M, Walton K, Ward A, Totea A-M, Taheri S, Mawla N, Adebisi AO, Elawad S, Diza C, Timmins P, Conway BR. Effect of preparation method on the surface properties and UV imaging of indomethacin solid dispersions. European Journal of Pharmaceutics and Biopharmaceutics. 2019;137:148-163.

36 Alqahtani, F., Belton, P., Ward, A., Asare-Addo, K., & Qi, S. (2020). An investigation into the use of low quantities of functional additives to control drug release from hot melt extruded solid dispersions for poorly soluble drug delivery. International Journal of Pharmaceutics, 2020;579 119172.

37. Ward A, Walton K, Mawla N, Kaialy W, Liu L, Timmins P, Conway BR, Asare-Addo K. Development of a novel method utilising dissolution imaging for the measurement of swelling behaviour in hydrophilic matrices. International journal of pharmaceutics: X. 2019;1:100013.

38. Madelung P, Bertelsen P, Jacobsen J, Müllertz A, Østergaard J. Dissolution enhancement of griseofulvin from griseofulvin-sodium dodecyl sulfate discs investigated by UV imaging. Journal of Drug Delivery Science and Technology. 2017;39:516-522.

39. Hiew TN, Alaudin MI, Chua SM, Heng PW. A study of the impact of excipient shielding on initial drug release using UV imaging. International Journal of Pharmaceutics. 2018 Dec 20;553(1-2):229-37.

40. Nokhodchi A, Homayouni A, Araya R, Kaialy W, Obeidat W, Asare-Addo K. Crystal engineering of ibuprofen using starch derivatives in crystallization medium to produce promising ibuprofen with improved pharmaceutical performance. RSC Advances. 2015;5(57):46119-46131.

41. Bučar DK, Elliott JA, Eddleston MD, Cockcroft JK, Jones W. Sonocrystallization Yields Monoclinic Paracetamol with Significantly Improved Compaction Behavior. Angewandte Chemie International Edition. 2015;54(1):249-253.

42. Di Martino P, Guyot-Hermann AM, Conflant P, Drache M, Guyot JC. A new pure paracetamol for direct compression: The orthorhombic form. International Journal of Pharmaceutics. 1996;128(1):1-8.

43. Walton K, Fleming L, Goodhand M, Racasan R, Zeng W. High fidelity replication of surface texture and geometric form of a high aspect ratio aerodynamic test component. Surface Topography: Metrology and Properties. 2016;4(2):25003.

44. Walton K, Blunt L, Fleming L. The topographic development and areal parametric characterization of a stratified surface polished by mass finishing. Surface Topography: Metrology and Properties. 2015;3(3):35003.

45. Walton K, Blunt L, Fleming L, Goodhand M, Lung H. Areal parametric characterisation of ex-service compressor blade leading edges. Wear. 2014;321:79-86.

46. Convention USP. First supplement to USP 42-NF37. In. Rockville, Maryland: United States Pharmacopeial Convention.; 2019.

47. Taylor Hobson UoH. Surfstand. In. Huddersfield; 2013.

48. Helmli F. Focus Variation Instruments. In. Berlin, Heidelberg: Springer Berlin Heidelberg; 2011. p. 131-166.

49. Al-Karawi C, Kaiser T, Leopold CS. A novel technique for the visualization of tablet punch surfaces: characterization of surface modification, wear and sticking. International Journal of Pharmaceutics. 2017 Sep 15;530(1-2):440-54.

50. Laity PR, Asare-Addo K, Sweeney F, Šupuk E, Conway BR. Using small-angle X-ray scattering to investigate the compaction behaviour of a granulated clay. Applied Clay Science. 2015;108:149-164.

51. Rose AA, Kaialy W. Improved tableting behavior of paracetamol in the presence of polyvinylpyrrolidone additive: Effect of mixing conditions. Particuology. 2019;43:9-18.

52. Khanmohammadi M, Garmarudi AB, Moazzen N, Ghasemi K. Qualitative Discrimination Between Paracetamol Tablets Made by Near Infrared Spectroscopy and Chemometrics With Regard to Polymorphism. Journal of Structural Chemistry. 2010;51(4):663-669.